A New Model System for Diffusion NMR Studies of Concentrated Monodisperse and Bidisperse Colloids

Swomitra Palit and Anand Yethiraj*

*Department of Physics and Physical Oceanography, Memorial University of Newfoundland,
St. John's. NL, Canada*

A method to prepare monodisperse and simultaneously NMR-visible and fluorescent colloidal particles is described, and a systematic approach to obtain spectrally resolved diffusion coefficient for every component in a monodisperse colloidal suspension is presented. We also prepared bidisperse colloidal suspensions, where each colloid component has a distinct NMR spectral signature, and obtained the diffusion coefficients of both colloid species simultaneously in concentrated colloidal suspensions, with volume fractions between 20 and 50%. The colloidal model system developed in this work enables the study of colloidal phase behavior in binary mixtures for different number and size ratios.

1. Introduction

Self-organization in suspensions of hard-sphere colloids closely mimics phase behavior in atomic fluids, forming colloidal fluids, close-packed crystals, and amorphous "glassy" solid structures[1] as well as numerous complex crystalline structures[2-8] (see ref 9 for a review). The entropic contribution to the colloidal free energy is richer in complexity when the colloidal "atoms" are bidisperse. In particular bidispersity can suppress crystallization and allow the dynamics of structural relaxation to fully develop. Associated with the glass transition is a theoretical prediction of the existence of a singularity of purely kinetic origin.[10] A recent success in the understanding of the glass transition is the theoretical and experimental discovery of a transition from an attractive to repulsive glass phase,[11] where the experimental study was done on a colloidal model system.

Many theoretical and computer simulation studies have focused on the study of phase behavior of bidisperse colloidal suspensions.[12-17] Stable, isostructural solid−solid as well as fluid−fluid transitions are expected.[14] Experiments on bidisperse colloidal systems have been carried out for various size ratios,[18-26]

but detailed comparisons of local dynamics as a function of size ratios and number ratios would be valuable.

Experimental studies of static and dynamical properties of colloidal suspensions have predominantly used light scattering[1] or optical (confocal) microscopy,[27] both in the optical single scattering limit (requiring samples to be optically transparent), although multiple scattering studies[28] as well as two-color techniques to suppress multiple scattering contributions[29,30] have yielded important information. Studies of concentrated, bidisperse colloidal suspensions present another challenge: how to extract dynamical information of each component in a model-independent manner? While the primary strength of confocal microscopy over scattering techniques is the model independence of the data analysis, the need to remain in the Brownian regime for colloidal suspensions limits the size ratio accessible to microscopy to about 3:1.

In this study, we present a new colloidal model system for pulsed-field-gradient (PFG) NMR studies of the colloidal dynamics on monodisperse and bidisperse colloidal suspensions. PFG NMR is a powerful tool to measure self-diffusion in complex fluids.[31,32] While PFG NMR techniques have been used to study colloidal suspensions,[33-35] the systems have either suffered from low signal strength or polydispersity large enough to prevent study of phase behavior. Moreover there are no reports of NMR studies on bidisperse colloids. Our methods allow simultaneous, model-independent measures of diffusion coefficients of all

* Corresponding author: E-mail: anand@physics.mun.ca.

(1) Pusey, P. N. In *Liquids, freezing and glass transition*; Hansen, J.-P., Levesque, D., Zinn-Justin, J., Eds.; North-Holland: Amsterdam, 1991; Chapter 10.

(2) Bartlett, P.; Ottewill, R. H.; Pusey, P. N. *Phys. Rev. Lett.* **1992**, *3801*, 68.

(3) Zahn, K.; Maret, G. *Phys. Rev. Lett.* **2000**, *85*, 3656.

(4) Yethiraj, A.; van Blaaderen, A. *Nature* **2003**, *421*, 513.

(5) Roichman, Y.; Grier, D. G. *Opt. Express* **2005**, *13*, 5434.

(6) Leunissen, M. et al. *Nature* **2005**, *235*, 437.

(7) Bartlett, P.; Campbell, A. I. *Phys. Rev. Lett.* **2005**, *128302*, 95.

(8) Shevchenko, E. V.; Talapin, D. V.; Kotov, N. A.; O'Brien, S.; Murray, C. B. *Nature* **2006**, *55*, 439.

(9) Yethiraj, A. *Soft Matter* **2007**, *3*, 1099.

(10) Götze, W. In *Liquids, freezing and glass transition*; Hansen, J.-P., Levesque, D., Zinn-Justin, J., Eds.; North-Holland: Amsterdam, 1991; Chapter 5.

(11) Poon, W. C. K. *J. Phys.: Condens. Matter* **2002**, *14*, R859.

(12) Barratt, J. L.; Latz, A. *J. Phys.: Condens. Matter* **1990**, *2*, 4289.

(13) Kob, W.; Anderson, H. C. *Phys. Rev. E* **1995**, *51*, 4626.

(14) Dijkstra, M.; van Roij, R.; Evans, R. *Phys. Rev. E* **1999**, *59*, 5744.

(15) Fof, G.; Götze, W.; Sciortino, F.; Tartaglia, P.; Voigtmann, Th. *Phys. Rev. E* **2004**, *69*, 011505.

(16) Flenner, E.; Szamel, G. *Phys. Rev. E* **2005**, *72*, 031508.

(17) Kikuchi, N.; Horbach, J. *Europhys. Lett.* **2007**, *77*, 26001.

(18) Imhof, A.; Dhont, J. K. G. *Phys. Rev. E* **1995**, *52*, 6344.

(19) Imhof, A.; van Blaaderen, A.; Maret, G.; Mellema, J.; Dhont, J. K. G. *J. Chem. Phys.* **1994**, *100*, 2170.

(20) Crocker, J. C.; Matteo, J. A.; Dinsmore, A. D.; Yodh, A. G. *Phys. Rev. Lett.* **1999**, *82*, 4352.

(21) Dinsmore, A. D.; Yodh, A. G.; Pine, D. J. *Phys. Rev. E* **1995**, *52*, 4045.

(22) Kaplan, P. D.; Yodh, A. G.; Pine, D. J. *Phys. Rev. Lett.* **1992**, *68*, 393.

(23) Sanyal, S.; Easwar, N.; Ramaswamy, S.; Sood, A. K. *Europhys. Lett.* **1992**, *18*, 107.

(24) Lekkerkerker, H. N. W.; Stroobants, A. *Physica A* **1993**, *195*, 387.

(25) Williams, S. R.; van Megen, W. *Phys. Rev. E* **2001**, *64*, 041502.

(26) Williams, S. R.; McGlynn, P.; Bryant, G.; Snook, I. K.; van Megen, W. *Phys. Rev. E* **2006**, *74*, 031204.

(27) van Blaaderen, A.; Wiltzius, P. *Science* **1995**, *270*, 1177.

(28) Pine, D. J.; Weitz, D. A.; Chaikin, P. M.; Herbolzheimer, E. *Phys. Rev. Lett.* **1988**, *60*, 1134.

(29) Segrè, P. N.; van Megen, W.; Pusey, P. N.; Schätzel, K.; Peters, W. *J. Mod. Opt.* **1995**, *1929*, 42.

(30) Segrè, P. N.; Pusey, P. N. *Physica A* **1997**, *232*, 9.

(31) Momot, K. I.; Kuchel, P. W. *Concepts Magn. Reson., Part A* **2006**, *28A*, 249.

(32) Callaghan, P. T. *Principles of Nuclear Magnetic Resonance Microscopy*, 1st ed.; Clarendon Press: Oxford, 1991.

(33) Blees, M. H.; Geurts, J. M.; Leyte, J. C. *Langmuir* **1996**, *12*, 1947.

(34) Wagner, J.; Härtl, W.; Walderhaug, H. *J. Chem. Phys.* **2001**, *114*, 975.

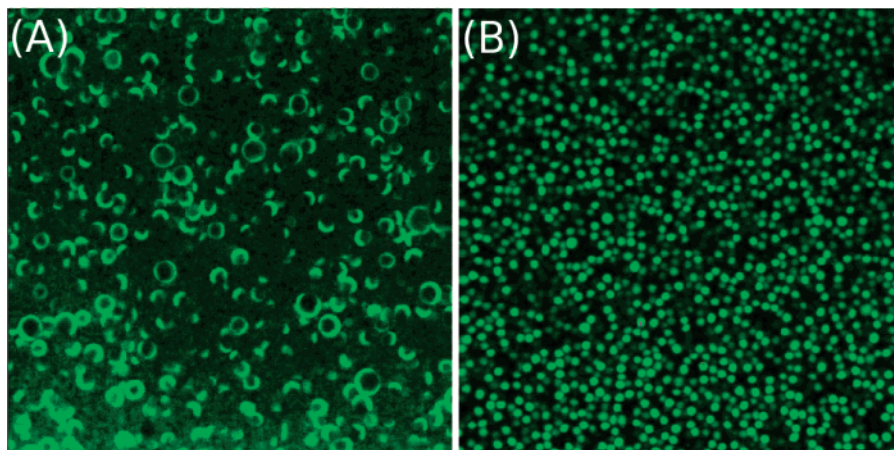(35) Wassenius, H.; Nydén, M.; Vincent, B. *J. Colloid Interface Sci.* **2003**, *264*, 538.

Figure 1. Confocal image of 0.99 μ spheres with the "oil" *p*-xylene (50% in ratio of the polystyrene volume) with coumarin-6 fluorophore (0.09%). (A) Initially all the fluorescent oil is seen as droplets in the water phase, with the polystyrene spheres being nonfluorescent. (B) After optimal ultrasonication conditions (see text) the particles were fluorescent and the aqueous medium nonfluorescent.

components of an opaque, multicomponent colloidal suspension with no fundamental limits on size ratio. We present diffusion coefficients for monodisperse polystyrene spheres of four sphere diameters as well as concentrated bidisperse colloidal suspensions at different volume fractions to demonstrate our methods and find that the smaller component is slowed down less on increasing packing fraction than the larger component.

2. Experimental Section

2.1. Preparation of NMR Visible and Fluorescent Colloids. Commercial monodisperse polystyrene spheres of different mean diameters (0.99 ± 0.1, 0.79 ± 0.03, 0.54 ± 0.05, and 0.25 ± 0.04 μ) purchased from Bangs Laboratories, sizes and polydispersities determined by us from SEM measurements, were modified to make them simultaneously NMR-visible as well as fluorescent, enabling us to characterize the particles with fluorescence laser scanning confocal microscopy prior to preparing the samples for NMR spectroscopy. Solid polystyrene has a broad NMR peak width and has extremely short relaxation times. It is thus unobservable in standard high-resolution NMR spin echo or stimulated echo experiments. Thus water-insoluble organic liquids (termed as "oil" in what follows) were added to polystyrene−water suspensions and ultrasonicated until all the oil was incorporated inside the polystyrene matrix. A water-insoluble fluorescent dye was added to the oil to simultaneously make the particles visible by confocal microscopy in order to optimize the ultrasonication times and temperatures.

Two such oil incorporations were devised. *p*-Xylene with 0.09% coumarin-6 dye was seen to be completely incorporated into polystyrene after ultrasonication for 25 min at 23 °C, and trimethylphenyl silane with 0.03% of nile red dye was seen to be completely incorporated into polystyrene after ultrasonication for 40 min at 30 °C. While prior to ultrasonication, the oil was observed in a highly polydisperse (and fluorescent) droplet form in the water medium, successful ultrasonication was judged by the absence of fluorescent droplets and, instead, the presence of monodisperse fluorescent spheres of the same size as the original polystyrene spheres (Figure 1). Moreover, the fluorescence in the spheres was observed to be very uniform. The amount of oil as well as ultrasonication time were adjusted to maximize oil incorporation (better at low oil concentrations) while trying to maximize the resulting NMR signals (better at high oil concentrations). The happy medium was found to be at an amount of the fluorescent-dyed oil corresponding to 50% of the total volume of spheres in the colloidal suspension. The incorporation of oil could be expected to cause swelling of the particle radius minimally ($\approx 1.5^{1/3}$). Measurements of particle diameter in solution via confocal microscopy are consistent with a $\approx 10\%$ increase in particle size.
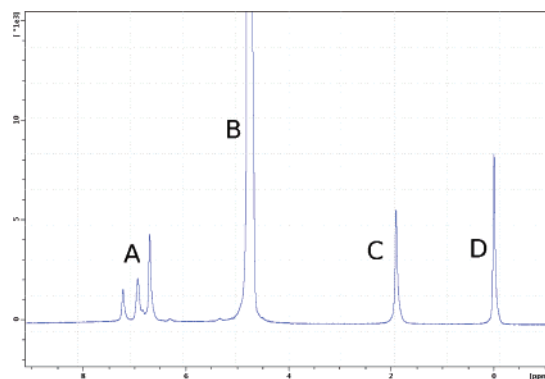

Figure 2. 1D spectrum of binary mixture of 0.99 μ spheres with trimethylphenyl silane ("0.99/tpmS") and 0.79 μ spheres with *p*-xylene ("0.79/pX"). The peaks are: (A) phenyl peaks from both *p*-xylene and trimethylphenyl silane, (B) water peak (top of peak truncated), (C) methyl peak of *p*-xylene, and (D) methyl peak of trimethylphenyl silane. C and D peaks are separated by 2 ppm.

The conductivity of the colloidal suspensions was measured to be in the range 2.9 ± 0.1 mS/cm, resulting in almost hard-sphere-like colloids.

Binary colloidal suspensions were prepared by mixing predetermined quantities of monodisperse suspensions, where the two colloidal components have different oils infused in them. Since *p*-xylene (pX) and trimethylphenyl silane (tpmS) have different NMR spectra (in particular, the methyl peak of trimethylphenyl silane and the methyl peak of *p*-xylene are separated by 2 ppm), the binary mixtures of colloids contain distinct NMR signatures for each component. In Figure 2, a Fourier transformed 1D spectrum of a binary colloidal suspension is shown. The set of peaks marked A are the overlapping phenyl peaks of the 0.99 μ particles with trimethylphenyl silane (0.99/tpmS) and the 0.79 μ particles with *p*-xylene (0.79/pX), while the C and D peaks correspond to the 0.79/pX and the 0.99/tpmS particles, respectively. The peak marked B is the water solvent peak (top of the peak has been clipped, as it is much higher). Thus *all* the components of the colloidal suspension are simultaneously spectrally resolved.

2.2. Diffusion NMR Measurements. Pulsed-field-gradient diffusion NMR measurements were carried out on a Bruker Avance II 600 spectrometer equipped with a Bruker 14.08 T magnet and a Bruker diffusion Diff30 probe (with a ^{1}H radiofrequency coil insert with an inner diameter of 5 mm) with a maximum Z gradient strength of 1800 G/cm (18 T/m). To avoid probe heating and to control sample temperature, the probe was cooled by flowing water and the temperature was maintained at 25 °C. Samples were prepared in 5 mm outer diameter NMR tubes.

Table 1. Relaxation Times and Ratios T_2/T_1 for Pure Solvents and for Solvents Incorporated into 0.99 μ Colloids

solvent	T_1^b (s)	T_2^b (ms)	T_1^c (s)	T_2^c (ms)	T_2^b/T_1^b	T_2^c/T_1^c	τ_C^c/τ_C^b
pX	1	150	1.9	40	0.15	0.02	2.5
tpmS	0.5	50	2	19	0.1	0.01	3.3

^{a} superscripts b and c stand for "bare" and "colloid", respectively.

In all samples, we obtain diffusion coefficients for the water and oil components simultaneously. We use a ^{1}H NMR pulsed-field-gradient stimulated echo pulse program[36] to measure diffusion: $(\pi/2)_x - \tau - (\pi/2)_x - (\Delta - \tau) - (\pi/2)_x - \tau -$ echo. Trapezoidal pulsed gradients of duration δ and peak amplitude g are applied during the τ durations 5 μs after the first and third $\pi/2$ pulses. The peaks of the trapezoidal gradient pulses are separated by the time Δ. A homogeneity-spoiling gradient of duration $\delta_{spoil} = 2$ ms, applied during the $\Delta - \tau$ duration 5 μs after the second $\pi/2$ pulse, removes unwanted transverse coherences during the Z storage time. The gradient steps were varied in 32 steps to a maximum gradient amplitude of 1600 G/cm for colloid diffusion and in 16 steps to 100 G/cm for water diffusion. The signal for each component as a function of gradient strength was obtained by integrating regions of the spectrum (obtained via a Fourier transform of the echo signal for each slice) that corresponded to different chemical species. Signal attenuation due to diffusion in the stimulated echo sequence is given by

$$S(g) = S_0 \exp(-\gamma^2 g^2 \delta^2 (\Delta - \delta/3)D) \quad (1)$$

where D is the self-diffusion coefficient. Therefore in a pulsed-field-gradient experiment, one can vary a generalized gradient strength parameter k, where $k = \gamma^2 g^2 \delta^2 (\Delta - \delta/3)$. A standard calibration sample (pure D_2O) was run prior to every set of experiments to ensure consistency between datasets.

In order to obtain adequate signal quality in NMR, one needs to perform signal averaging. For example, for monodisperse suspensions at volume fractions $\phi = 10\%$ and $\Delta = 100$ ms, signal averaging of 64 scans was employed, and the total experimental time was ≈ 3 h. For $\Delta = 500$ ms, experiments on the same sample required signal averaging of 256 scans, and hence the total experimental time was ≈ 12 h. Experimental times are longer for larger Δ but shorter for higher volume fractions.

2.3. Relaxation Measurements. Longitudinal relaxation time T_1 and transverse relaxation times T_2 were measured for each of the pure solvents (pX and tpmS) as well as for each solvent incorporated into 0.99 μ colloids. Assuming that relaxation occurs due to dipole–dipole interactions, we obtain a form for the ratio (T_2/T_1) as a function of the correlation time τ_C that is independent of atomic parameters but simply a ratio of two spectral density factors:[37]

$$\frac{T_2}{T_1} = 2 \frac{j(\omega_0) + j(2\omega_0)}{3j(0) + 5j(\omega_0) + 2j(2\omega_0)} \quad (2)$$

where $j(\omega) = (\tau_C)/(1 + \omega^2 \tau_C^2)$ and ω_0 is the proton Larmor frequency (600 MHz). From this ratio for each set of T_1 and T_2 measurements, we can obtain a correlation time τ_C. Then using the Stokes–Einstein relation for molecular diffusion $D = k_B T/6\pi\eta a_{mol})$ and the relation between the correlation time and the ideal bulk molecular diffusion in a homogeneous medium $\tau_C = 2a_{mol}^2/2D$, we can obtain viscosities $\eta = \tau_C(k_B T/12\pi a_{mol}^3)$. Indeed, we can remove the dependence on molecular size by taking ratios of values for oil inside oil-infused colloids and the bare values of the oils, yielding

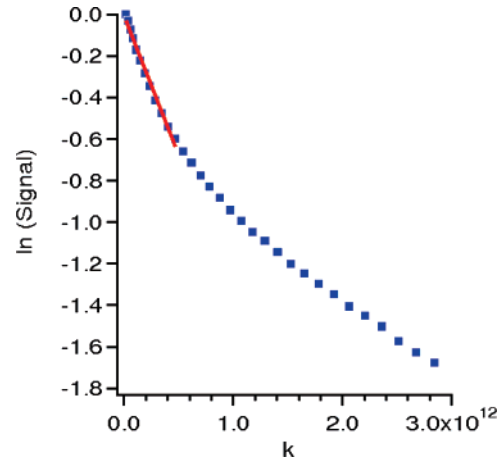$$\frac{\eta^c}{\eta^b} = \frac{\tau_C^c}{\tau_C^b} \quad (3)$$

(36) Tanner, J. E. *J. Chem. Phys.* **1970**, *52*, 2523.

Figure 3. Signal attenuation curves for for 0.99/pX colloidal suspension (10% concentration). $\Delta = 100$ ms, $\delta = 2$ ms, $g_{max} = 1000$ G/cm. The slope of $\ln(S(g))$ at small gradients (and large Δ) can be fit to the form $(-d^2/(5\Delta))k$ for spherical restrictions, where d would be the radius for a spherical restriction (ref 32, p 374).
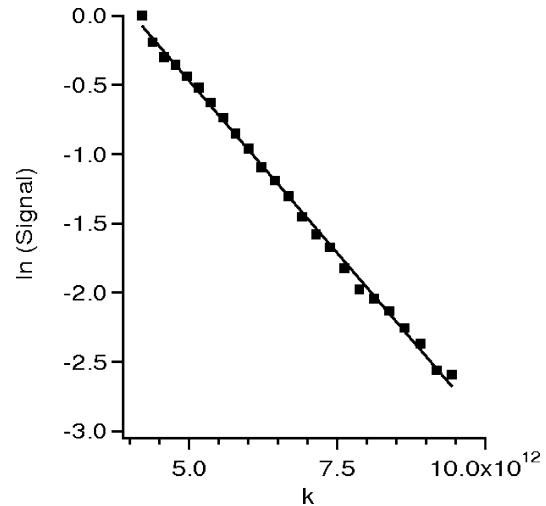

Figure 4. Same as Figure 3 but with $\Delta = 300$ ms. At large gradient $\ln(S(g))$ is linear and corresponds to the apparent colloid diffusion for the diffusion time probed.

From Table 1 it is clear that this ratio is roughly equal to 3. This is discussed in context with the results from diffusion in the Discussions and Conclusions section.

3. Results

3.1. Diffusion Coefficients in Monodisperse Suspensions. Signal attenuation of the oil in the polystyrene spheres was seen to consist of two distinct regimes: the fast restricted diffusion of the pX or tpmS within the sphere and the slow diffusion of the sphere itself. This is shown in Figure 3. For $k < 5 \times 10^{11}$ s^2/m, we probe the (relatively) fast restricted oil diffusion inside the sphere.

For $\Delta \gg d^2/2D_{oil}$, where D_{oil} is the bulk self-diffusion coefficient of the organic liquid (pX or tpmS, of the order of 10^{-9} m^2/s) and d is the radius of the (assumed spherical) restriction, the signal attenuation has the form[32] $S(g) = \exp(-kd^2/(5\Delta))$. Fitting the slope of $\ln(S(g))$ for $k < 5 \times 10^{11}$ s^2/m to a straight line (Figure 3), we obtain a restriction radius of 0.8 μ (for 0.99 μ spheres), 0.73 μ (for 0.79 μ spheres), and 0.36 μ (for 0.54 μm spheres), which is comparable to the particle diameter.

(37) Levitt, M. H. *Spin Dynamics*, 1st ed.; John Wiley and Sons: Chichester, 2001; Chapter 16.
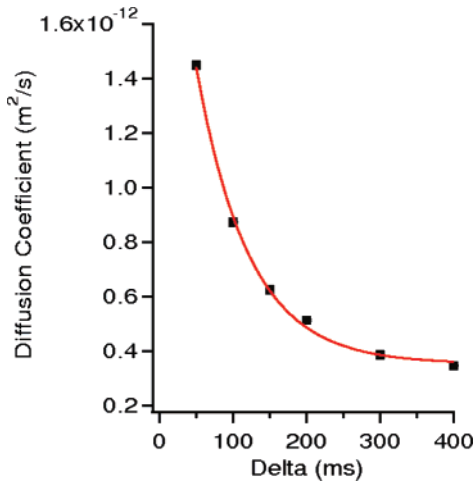
Figure 5. Plot of apparent diffusion coefficient as a function of diffusion time for 0.99 μ spheres in a $\phi = 20\%$ binary mixture. Here $\Delta = 50-400$ ms, $\delta = 1.88$ ms, and $g_{max} = 1200$ G/cm. The data fit well to an exponential fit, which is $D_{app} = D_{colloid} + A \exp(-\Delta/\tau_B)$. The plateau value yields the true colloid diffusion coefficient $D_{colloid}$. Errors in each data point are smaller than the symbols.

Figure 4 shows the logarithm of the signal attenuation vs the gradient strength parameter for large values, where $4 \times 10^{12} < k < 9.5 \times 10^{12} s^2/m$. Here the behavior is indeed linear and suggestive of colloid diffusion. However, the diffusion coefficient (referred to here as D_{app}) is dependent on Δ as shown in Figure 5. This apparent diffusion coefficient is large for diffusion times $\Delta < \tau_B$, where $\tau_B \approx a^2/6D_0$ is the Brownian time of the colloidal particle and D_0 is the Stokes−Einstein value of the colloid diffusion coefficient (valid at infinite dilution):

$$D_0 = \frac{k_B T}{6\pi\eta a} \tag{4}$$

where η is the solvent viscosity and a is the sphere radius. In addition, the rotational correlation time of the colloidal particles $\tau_r = (2/9)a^2/D_0$ (≈ 100 ms for 0.99 μ spheres). This implies that on this timescale particle rotations can contribute the apparent diffusion coefficient as well. The diffusion coefficient plotted against Δ however reaches a plateau value for $\Delta > \tau_B, \tau_r$, and we fit the dependence to a phenomenological form

$$D_{app} = D_{colloid} + A \exp\left(\frac{-\Delta}{\tau_B}\right) \tag{5}$$

with $D_{colloid}$ being interpreted as the true colloid diffusion coefficient. Since the diffusion time is on the same timescale as the interaction time $\tau_I \approx (2a)^2/D_0$ (often defined as the time taken for a particle to diffuse a distance equivalent to the position of the first peak of the pair correlation function), we interpret this as the short time self-diffusion coefficient.

The diffusion coefficient for colloidal suspensions (and its uncertainty) for different sizes of spheres was obtained from the plateau value of the exponential fit (and the standard deviation of the fitted value) from data such as that in Figure 5. In Figure 6, the measured colloid diffusion values $D_{colloid}$ for different particle sizes (diameter $2a$) are compared with the Stokes−Einstein prediction (eq 4). The dashed curve is for infinite dilution, while the solid curve is the corrected functional form for the short-time self-diffusion coefficient using hydrodynamic theory
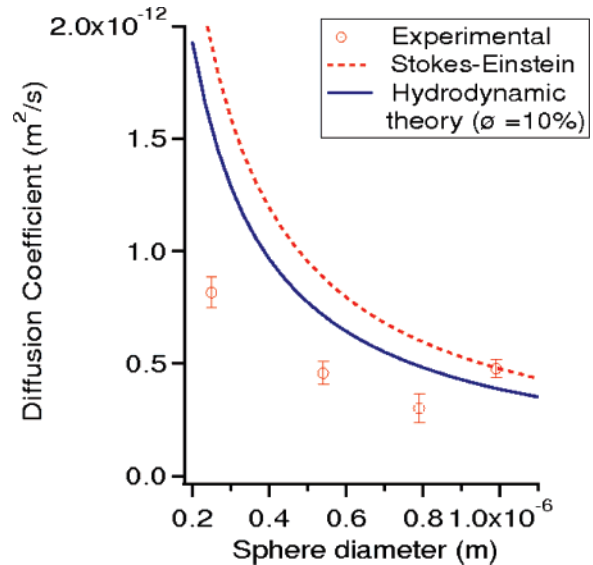
$$D_s^S = D_0(1 + k_s^S \phi) \tag{6}$$

Figure 6. Plot of diffusion coefficient $D_{colloid}$ vs particle diameter. Drawn curves show the Stokes−Einstein prediction (dashed curve, eq 4) and the hydrodynamic correction for the experimental volume fraction (solid curve) using eq 6 with $k_s^S = -1.73$.[38]

with $k_s^S = -1.73$[38] for a finite volume fraction ϕ of the suspensions. The diffusion coefficients measured show systematic deviations from the latter value. On the other hand, repeated experiments (carried out for colloidal suspensions at $\phi \approx 10\%$) yield reproducible values (within shown error bars) for the diffusion coefficient. Therefore, when studying concentrated colloidal suspensions, we compare diffusion coefficients that are scaled with respect the ones measured for the $\phi \approx 10\%$ monodisperse suspensions.

It is important to note the limitations of our technique. Signal strength is determined both by the amount of oil and the relaxation times T_1 and T_2. In all our samples, this meant that the signals were poor in samples with volume fractions less than 8% . Thus only the results for volume fractions 10% and above are reported. By the same token, the signal strength improved dramatically on increasing volume fraction.

3.2. Diffusion Measurements in Bidisperse Suspensions. For the binary mixture, we obtained simultaneous signal attenuation for both large and small particles and thus the diffusion coefficients of the two species simultaneously. In order to correct for systematic errors in the absolute measure of diffusion coefficient, we divide the results for each colloid species by the value of the diffusion coefficient for $\phi \approx 10\%$ monodisperse suspension of that species. We plot this scaled diffusion coefficient vs total volume fraction ϕ (Figure 7). Both components in the colloidal mixture are slowed down with increasing volume fraction. The slowing down of diffusion as a function of volume fraction is systematically more pronounced for the large spheres. This is in contrast to the results for long time self-diffusion coefficients of Imhof et al.[18] in bidisperse suspensions at large size ratios, where the slowing down of the scaled diffusion coefficients is identical for small and large spheres. On the other hand, Williams et al.[25] found in a binary system with size ratio of 1.7 that at constant total volume fraction ($\phi = 58\%$) increasing the partial fraction of small spheres increases the mobility of the spheres, resulting eventually in melting of the glass phase. These behaviors can all be tested in detail in our model system, and such experiments are currently under way.
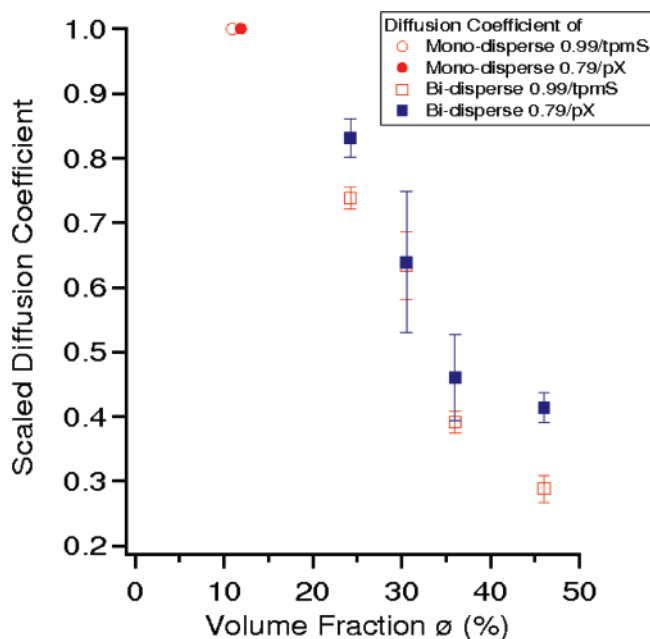
(38) Muthukumar, M.; Freed, K. F. *J. Chem. Phys.* **1983**, *78*, 497.

Figure 7. The scaled diffusion coefficient of both large and small spheres in binary mixture as a function of total particle volume fraction is shown. For 0.99/tpmS spheres, all values of diffusion coefficients are rescaled to that of 10.9% monodisperse suspension, and for 0.79/pX spheres, all values of diffusion coefficients are rescaled to that of 11.9% monodisperse suspension. All samples contain equal volume fractions of small and large spheres. Increasing volume fractions are prepared by centrifugation of the same sample to minimize systematic errors. Circles/squares represent monodisperse and bidisperse suspensions respectively. Filled/open symbols refer to 0.79/0.99 μ particles, respectively.

4. Discussions and Conclusions

We have designed a novel experimental model system for the study of dynamics in colloidal phases. Three previous PFG NMR experiments on spherical colloids are known to us. Wagner et al.[34] measured long-time self-diffusion coefficients in dilute suspensions (8% volume fraction). Blees et al.[33] also measured long-time self-diffusion coefficients at volume fractions between 4 and 25%. Both these techniques used the signal from the polymer in the colloid itself. In a stimulated echo experiment, where diffusion time is a variable of interest, signal strength is inversely related to the natural NMR line width, which in turn is broader for solidlike materials. The work of Wassenius et al.[35] used liquid-core particles to increase signal strength, but the system was highly polydisperse (with a size range from 1 to 8 μm). None of these systems was directly usable for bidisperse colloids.

We have demonstrated particle preparation/synthesis techniques to make monodisperse colloids with absorbed organic liquids and thus have both controllable NMR signatures (Figure 2) as well as fluorescent dye (Figure 1). The latter, along with SEM, allows us to characterize the particles synthesized and ensure inclusion of the oil inside the particles, while the former provides us with the means to study bidisperse colloids via diffusion NMR. The NMR signal attenuation consisted of a low-gradient strength behavior that corresponds to restricted diffusion of the organic liquid inside the polystyrene matrix (Figure 3) and a high-gradient strength behavior that resulted from colloid motion (Figure 4). If the colloid motion was a simple Brownian translational diffusion, the diffusion coefficient thus obtained from Figure 3 would be independent of diffusion time Δ. However, when $\Delta \approx 100$ ms (for the 0.99 μm spheres), it is comparable to both the typical Brownian timescales τ_B as well as the colloid rotational correlation times τ_r. The apparent diffusion

coefficient however was found to be a function of Δ (Figure 5), and this function was well fit by a phenomenological exponential form, with the constant being the plateau value and identifiable as the colloid translational diffusion coefficient. Since the Δ values probed are on the same order as the Brownian time, this corresponds to the short time self-diffusion coefficient. We have not yet reached fundamental limits in terms of the diffusion times we can probe. Preliminary experiments suggest easy extension of the range of Δ values accessible to 5 s. We can also probe smaller colloidal spheres (thus increasing Δ/τ_B) using our method. This will allow us to explore timescales between the short-time and the long-time limits.

There are three observations that convince us that the oil is indeed resident inside the particles: these are, first, the monoexponential large k behavior; second, the diffusion coefficient bounded by the ideal Stokes−Einstein diffusion value; and third, the complementary confocal imaging of fluorescent-dyed oil. We observe, however, a discrepancy between the apparent viscosity deduced from diffusion measurements and from relaxation measurements. The effective diffusion coefficient of oil inside the polystyrene colloid is affected by the size restriction presented by the colloid. This measured value ($\approx 10^{-12}$ m^2/s) is a lower limit for the diffusion of the oil in bulk polystyrene. This thus sets an upper limit for the effective viscosity seen by the diffusing oil of $1000 \times \eta^b$ (where η^b is the "bare" viscosity of the oil). If the oil were diffusing in a homogeneous medium, the effective viscosity as obtained from the diffusion coefficient via the Stokes−Einstein relation would equal the viscosity obtained from relaxation. However, the latter is much smaller ($\approx 3 \times \eta^b$). Therefore, we must conclude that the colloid is not resident in a homogeneous porous medium. We conjecture that a heterogeneous network of interconnected pores could result in a lower effective diffusion coefficient. A detailed study of relaxation at different field frequencies and of diffusion in bulk polystyrene is planned.

We plot the diffusion coefficients for monodisperse colloidal suspensions at a single volume fraction for four particle sizes (Figure 6). We find that the diffusion coefficients are close to the value expected from the Stokes−Einstein relation corrected for hydrodynamic interactions. However, there do exist systematic deviations, which we are currently trying to understand. We then measured diffusion coefficients in bidisperse colloidal suspensions with equal volume fractions of small and large spheres. We began with a colloidal suspension at $\phi = 20\%$ (corresponding to a partial volume fraction of each component of $\approx 10\%$) and made more concentrated suspensions by successive centrifugation without removing from the sealed NMR tube. At four volume fractions, we then measured diffusion coefficients of both components simultaneously. We found that the scaled diffusion coefficient (the diffusion coefficient of each colloid species in the binary mixture scaled with its value in the $\approx 10\%$ monodisperse suspensions) shows a systematic decrease by more than a factor of 2 (Figure 7) when the total volume fraction is varied between 20 and 50%. The small spheres appear to have slowed down less than the large spheres.

Detailed measurements of diffusion coefficients in concentrated bidisperse colloidal suspensions at different size ratios and number ratios are currently under way.